OPTICA

High-sensitivity SNSPD-enabled swept source Raman spectroscopy for cancer detection with SERS nanoparticles

Yifan Liu,[1,2] A. K. M. Atique Ullah,[2,3] Timothy M. Rambo,[4] Aniwat Juhong,[1,2] Bo Li,[1,2] Cheng-you Yao,[2,5] Min Li,[1,2] Jeremy S. Doredla,[4] Stephanie Boyd,[4] Gary D. Luker,[6] Ming Han,[1] Aaron J. Miller,[4] Xuefei Huang,[2,3,5] and Zhen Qiu[1,2,5,*]

[1]Department of Electrical and Computer Engineering, Michigan State University, East Lansing, Michigan 48824, USA
[2]Institute for Quantitative Health Science and Engineering, Michigan State University, East Lansing, Michigan 48824, USA
[3]Department of Chemistry, Michigan State University, East Lansing, Michigan 48824, USA
[4]Quantum Opus, LLC, Plymouth, Michigan 48170, USA
[5]Department of Biomedical Engineering, Michigan State University, East Lansing, Michigan 48824, USA
[6]Departments of Radiology and Biomedical Engineering, University of Michigan, Ann Arbor, Michigan 48109, USA
*qiuzhen@msu.edu

Received 3 June 2025; revised 20 September 2025; accepted 6 November 2025; published 18 December 2025

Highly sensitive and specific molecular detection is essential for advancing early cancer diagnosis. In this paper, we present an imaging system that combines swept source Raman spectroscopy with surface-enhanced Raman scattering (SERS) nanoparticles to enhance cancer detection capability. By incorporating a high-efficiency superconducting nanowire single-photon detector (SNSPD), the system achieves remarkable detection sensitivity to the femtomolar concentrations. This performance was demonstrated under practical conditions using only 30 mW excitation power and 40 ms wavelength point exposure time, enabling ultra-sensitive acquisition. Imaging experiments on both cell and tissue samples confirm the system's compatibility with various biological applications. Combining high sensitivity, speed, and specificity, this platform offers a promising approach for molecular imaging and early stage cancer detection using SERS-based probes.

https://doi.org/10.1364/OPTICA.569117

A nationwide 77% increase in new cancer cases is projected by 2050 compared to 2020, according to GLOBOCAN [1], highlighting the critical need for more accurate and efficient cancer detection techniques. Traditional methods like H&E slides preparation and pathology annotation are time-consuming and labor-intensive, making them insufficient to meet growing clinical demands. As a result, there is increasing interest in technologies capable of providing rapid, real-time diagnostic information. Raman spectroscopy, an optical method providing a molecular-level fingerprint of samples through the inelastic light scattering is one of the promising choices of cancer detection since early 1990s [2]. However, the weak intrinsic Raman signal typically requires high excitation laser power and long exposure time, limiting its wide clinical use.

To address these challenges, surface-enhanced Raman spectroscopy (SERS) was developed. By incorporating the chemical component with nanostructured metal surfaces, SERS could amplify the Raman signals by factor from 10^4 to 10^8 [3]. Therefore, SERS largely reduced required exposure time and enabled detection at low concentrations. Furthermore, when conjugated with molecular biomarkers, SERS nanoparticles (SERS NPs) become powerful tools for targeted cancer diagnosis [4].

While SERS significantly improves signal intensity, the effectiveness of the Raman system still relies on the optical architecture. Among various Raman spectroscopies, the dispersive Raman spectroscopy remains the most common architecture. In this spectroscopy, a diffraction grating spatially resolves the Raman signal onto a line-scan camera. Despite its wide use, this conventional approach faces some limitations, including relatively low light collection efficiency, interference from fluorescence, and the large size and cost of high-performance cameras. These limitations constrain its sensitivity and potential for miniaturization.

To overcome these limitations, an alternative architecture known as swept source Raman spectroscopy (SSRS) has been developed. At the early stage, researchers replaced the fixed-wavelength laser source with a tunable laser source, while still utilizing the line camera to capture the two-dimensional Raman spectra [5]. More recently, over the past five years, researchers have started to integrate the single-point detector into the SSRS [6]. In this configuration, a narrow bandpass filter is placed in front of a sensitive detector, only allowing the photons with a specific wavelength range to be detected. As the tunable excitation laser sweeps across a range of wavelengths, the relative Raman shift of the detected photons changes accordingly. The complete Raman spectrum could be reconstructed by recording the signal intensity as a function of the excitation wavelength. This architecture, which replaces the slit, diffraction grating, and camera, significantly enhances light collection efficiency and allows for system miniaturization. The new SSRS configuration has been already applied

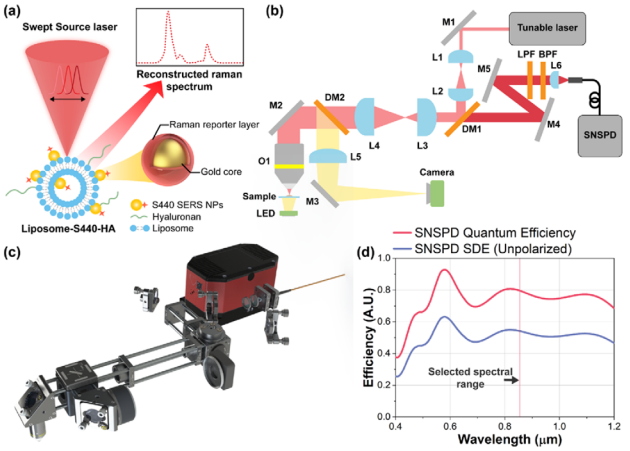

Fig. 1. Superconducting nanowire single-photon detector-based swept source Raman spectroscopy setup. (a) Conceptual drawing of the swept source Raman spectroscopy applied to Liposome-S440-HA, including the targeted SERS nanoparticle's structural composition. (b) Schematic of the SNSPD-SSRS: L1–L6, lenses; DM1–DM2, dichroic mirrors; M1–M5, reflective mirrors; O1, objective lens; LPF, long-pass filter; and BPF, bandpass filter. (c) CAD model of SNSPD-SSRS and (d) quantum efficiency and system detection efficiency of the large-area SNSPD detector used to collect the Raman scattering signal from SERS NPs.

in various domains including biomedical imaging [7,8], chemical identification [9,10], and environmental monitoring [11].

However, there are several critical gaps that remain unaddressed. First, no prior work has attempted to integrate a high-sensitivity detector into SSRS to enhance detection efficiency to a level comparable to or even exceeding that of dispersive Raman systems. Second, only a limited number of studies have employed fiber-coupled detectors, which is critical for further miniaturization. Finally, to our knowledge, no group has systematically conducted imaging experiments with SSRS, particularly in combination with SERS techniques.

In this paper, we propose a novel system: superconducting nanowire single-photon detector-based swept source Raman spectroscopy (SNSPD-SSRS). This system integrates a fiber-coupled superconducting nanowire single-photon detector (SNSPD), a leading-edge technology known for its high sensitivity and low background noise, with increasing applications in the biomedical imaging area [12]. Being compared to the conventional Raman spectroscopy, the SNSPD-SSRS enables the detection of Raman signal with lower excitation power and shorter wavelength point exposure time. This improvement is critical for accurate and rapid detection of SERS nanoparticles bound to tumor tissues, offering a promising tool for high-sensitivity cancer detection.

The overall system design and principle of SNSPD-SSRS with SERS NPs are illustrated in Fig. 1. Figure 1(a) is the working principle of the off-resonance SERS technique; the laser source firstly induces high local electromagnetic field region near the targeted SERS nanoparticle (Liposome-S440-HA), generating enhanced Raman scattering. The scattering signal is then filtered and captured by a large-area, multimode fiber-coupled, SNSPD device developed by Quantum Opus LLC. As the excitation wavelength sweeps, the SNSPD would sequentially capture signals across the whole spectrum range. Further information related to the signal reconstruction is provided in Fig. S1 of Supplement 1.

Figures 1(b) and 1(c) are optical schematic and CAD model of the SNSPD-SSRS system. The laser beam from the tunable laser (TLB-6712, Newport) would be firstly expanded by lenses L1 and L2 and further expanded by L3 and L4 after reflected by a dichroic mirror DM1 (FF801-Di02 − 25 × 36, Semrock). The expanded beam then passes DM2 (FF757 − Di01 − 25 × 36, Semrock) and fills the back pupil of the objective lens to excite the Raman scattering from SERS NPs. The scattered Raman signal is collected by the same objective lens and retraces the excitation path, passed back through DM2, L4, L3, and DM1. Two mirrors are used to align the scattering signal. A long-pass filter (BLP01-830 R-25, Semrock) and an ultra-narrow bandpass filter (855.625-0.75 OD6, Alluxa) are selected to eliminate the excitation laser light and select the scattering photon at a narrow spectral band from 855.25 to 856 nm. Finally, the filtered signal would be coupled by L6 into a multimode fiber (M67L02, Thorlabs), which was connected to a custom 30 μm core, graded-index fiber. This fiber was directly coupled to the large-area SNSPD device. A time tagger (Time Tagger Ultra, Swabian instruments) was used to record the pulse signals generated by the large-area SNSPD device.

The theoretical quantum efficiency and specified system detection efficiency (SDE) of the large-area SNSPD device across the range from 400 to 1200 nm are presented in Fig. 1(d). A narrow red box highlights the selected spectral window for SNSPD-SSRS in this study, where the SNSPD achieves a high SDE of approximately 55% for unpolarized photons. This high efficiency within the targeted wavelength range makes the SNSPD an excellent choice for detecting weak Raman scattering signals. Additionally, the SNSPD device can be further customized to achieve 90% SDE under optimized polarization, maximizing photon collection efficiency.

SERS nanoparticles of type S440 were selected for the SNSPD-SSRS imaging experiments. Detailed information of the S440 NPs is available in a previous publication [13]. Fundamental performance evaluations were conducted using the SNSPD-SSRS system, and the results are presented in Fig. 2. Figure 2(a) shows the Raman spectrum of S440 collected using a commercial dispersive Raman spectrometer with a 785 nm excitation, covering a Raman shift range from 500 to 2500 cm^{-1}. Then the orange-shaded region highlights the spectral range targeted by the SNSPD-SSRS. Given the tunable laser source range from 765 to 781 nm, the corresponding Raman shift range covered by SNSPD-SSRS is 1116.7 − 1384.5 cm^{-1}. It includes two major Raman peaks of S440 NPs at approximately 1200 cm^{-1} and 1340 cm^{-1} and one weak peak at 1237 cm^{-1}, ensuring that key spectral features can be captured and utilized in subsequent intensity-based map analysis.

To demonstrate that the SNSPD-SSRS could resolve and reconstruct the spectrum like the conventional dispersive Raman, we evaluated two different laser sweeping step sizes with S440 NPs, and the results are shown in Fig. 2(b). The red curve represents the example spectrum acquired from the commercial Raman system, while the other curves represent the SNSPD-SSRS data collected with 0.16 and 0.8 nm sweeping step sizes. Obviously, the 0.16 nm sweeping step size accurately reconstructed all three Raman peaks, including the weak peak at 1237 cm^{-1}. In contrast, the 0.8 nm sweeping step size failed to resolve this small feature.

To demonstrate the high detection efficiency enabled by the large-area SNSPD device, we tested the S440 NPs at a concentration gradient from 62.5 to 500 fM. The collected spectra are shown in Fig. 2(c). SNSPD-SSRS system was able to detect the 1340 cm^{-1} Raman peak at concentrations as low as 125 fM, and the 1200 cm^{-1} peak remained visible even at 62.5 fM. In contrast, the detection limit of the commercial Raman system was restricted to 250 fM under the same laser power and wavelength point

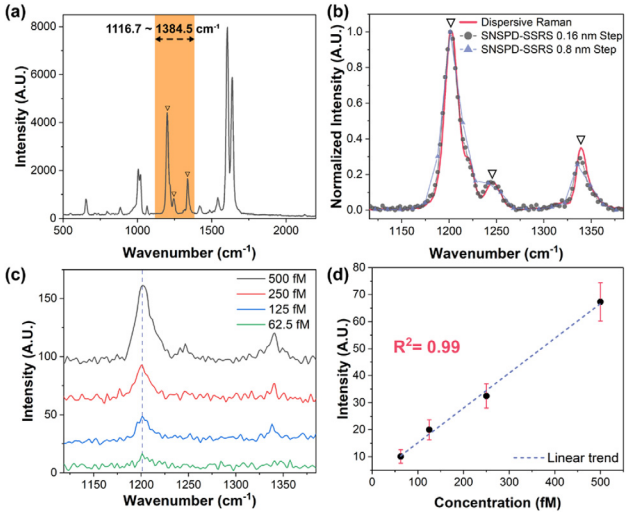

Fig. 2. Characterization experimental results of the SNSPD-SSRS on S440. (a) Reference curve of S440 captured by dispersive Raman spectroscopy. (b) The collected signal comparison between dispersive Raman and swept source Raman on S440 inside the orange range in (a). (c) Signal characterization of the S440 in four concentrations, the detection limit of SNSPD-SSRS is around 62.5 fM for S440. (d) The relative intensities of the 1200 cm^{-1}peak correlated linearly with S440 solution concentrations.

exposure time conditions. These results highlight the superior sensitivity of the SNSPD-SSRS system. Figure 2(d) illustrates a linear correlation between the intensity of the 1200 cm^{-1} peak and S440 NP concentration, confirming the quantitative detection capability of the system at low signal levels. The enhanced performance is attributed to the integration of the large-area SNSPD device, with a performance comparison of different SNSPD devices provided in Fig. S2 of Supplement 1. Additional experimental results provided in Fig. S3 of Supplement 1 illustrate the relationship between wavelength point exposure time, background noise, and Raman signal quality. As expected, longer wavelength point exposure times help sharpen the spectrum peaks detected by improving the signal-to-noise ratio.

To validate its applicability in practical biological sample imaging, we selected a 4T1 mouse breast tumor model for demonstration. To achieve specific targeting of the biological receptor CD44 overexpression on mice tumor cells, hyaluronan (HA) [14] was conjugated to liposome encapsulated S440 to form liposome-S440-HA. This targeted probe actively binds to CD44-overexpressing tumor regions, enabling clear differentiation between breast cancer and normal cells.

We began by evaluating the SNSPD-SSRS with the 4T1 breast cancer cell. The 4T1 cells were cultured on a quartz coverslip (043210.KJ, Thermo Fisher Scientific) for two days, then fixed and incubated with 100 pM liposome-S440-HA. After incubation, unbound nanoparticles were removed by rinsing with PBS, and the coverslip was mounted on a 2D motorized linear stage (MFA-CC08, Newport) for SNSPD-SSRS imaging. A 40× water immersion objective lens was used to enhance resolution for cellular imaging. An LED was utilized to illuminate the cells and guide the scanning area. The imaging results are displayed in Fig. 3.

Figure 3(a) is the representative wide-field image of 4T1 cells. The red-dashed box indicates the actual scanning region, covering an area of 78 by 108 μm with a step size of 3 μm. At each scan position, the reconstructed Raman spectrum was recorded, and the relative intensities of the 1200 and 1340 cm^{-1} peaks were

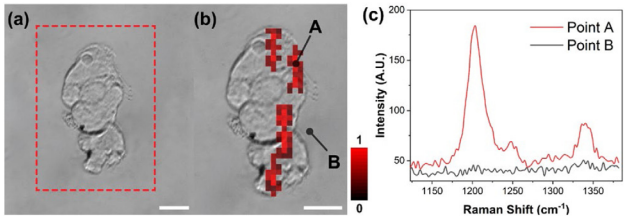

Fig. 3. Representative SNSPD-SSRS imaging of 4T1 cells incubated with lipsome-S440-HA. (a) Wide-field image of 4T1 cells, and red-dashed box represents the scanning region. (b) Overlap image of SERS intensity map and wide-field image of 4T1 cells. Points A and B mark representative locations on a targeted cell and background region, respectively. (c) Representative Raman signal from cell and background highlighted in (b). Scale bar: 20 μm.

calculated to generate a SERS intensity map after the scanning. Figure 3(b) is an overlay of the widefield image, and the SERS intensity map after a threshold was applied to remove the background unbound liposome-S440-HA signal. The Raman signal was clearly localized to the cell area, demonstrating selective targeting of 4T1 cells by liposome-S440-HA. The representative Raman spectra from targeted cell and background (marked as points A and B) are shown in Fig. 3(c). The high signal-to-noise ratio of the obtained spectrum (Point A) reflects both the high sensitivity of our SNSPD-SSRS system and the effective targeting of lipsome-S440-HA.

To further validate the practical utility of the SNSPD-SSRS system, we applied it to tumor tissue imaging using a 4T1 orthotopic mouse breast tumor model. The model was prepared by injecting the 4T1 cells into mammary fat pad of BALB/c mice. Tumor growth was monitored until the diameter exceeded 5 mm, at which point the mice were euthanized, and the tumor tissues were harvested for SNSPD-SSRS imaging. All animal procedures related to tissue imaging were approved by the Institutional Animal Care & Use Committee (IACUC) of Michigan State University.

The heart tissue from the same mouse bearing the breast tumor was also harvested as a control. Both the tumor and heart tissues were dissected to similar sizes and incubated with 100 pM liposome-S440-HA solution. Following incubation, the tissues were rinsed twice with PBS to remove unbound liposome-S440-HA. After sample preparation, the tissues were mounted on an aluminum plate fixed to the 2D stage and scanned by the SNSPD-SSRS system. The scanning results are presented in Fig. 4.

A photographic image of the tumor and heart tissue is shown in Figs. 4(a) and 4(b), and Figs. 4(c) is the corresponding SERS intensity map generated from Raman signal of lipsome-S440-HA. The scan covered an area of 11 mm × 7 mm with a 0.2 mm step size, using a 20× dry objective lens. The laser power applied to tissue sample scanning was 30 mW. The SERS intensity map clearly shows that bright Raman signals are mostly localized within the tumor region, while the signal detected from the heart tissue is relatively weak. Representative Raman spectra were collected from selected locations (Points A and B) on the tumor and heart tissues, as shown in Fig. 4(c). A further comparison between the breast tumor and healthy mammary tissue presented in Fig. S4 also supports this finding.

Following the imaging experiments, all the tissue samples were processed for histological analysis. For each tissue, we prepared the hematoxylin and eosin stain (H&E) and immunohistochemical (IHC) CD44 slides. The IHC-CD44 staining was specifically performed to validate CD44 overexpression in the

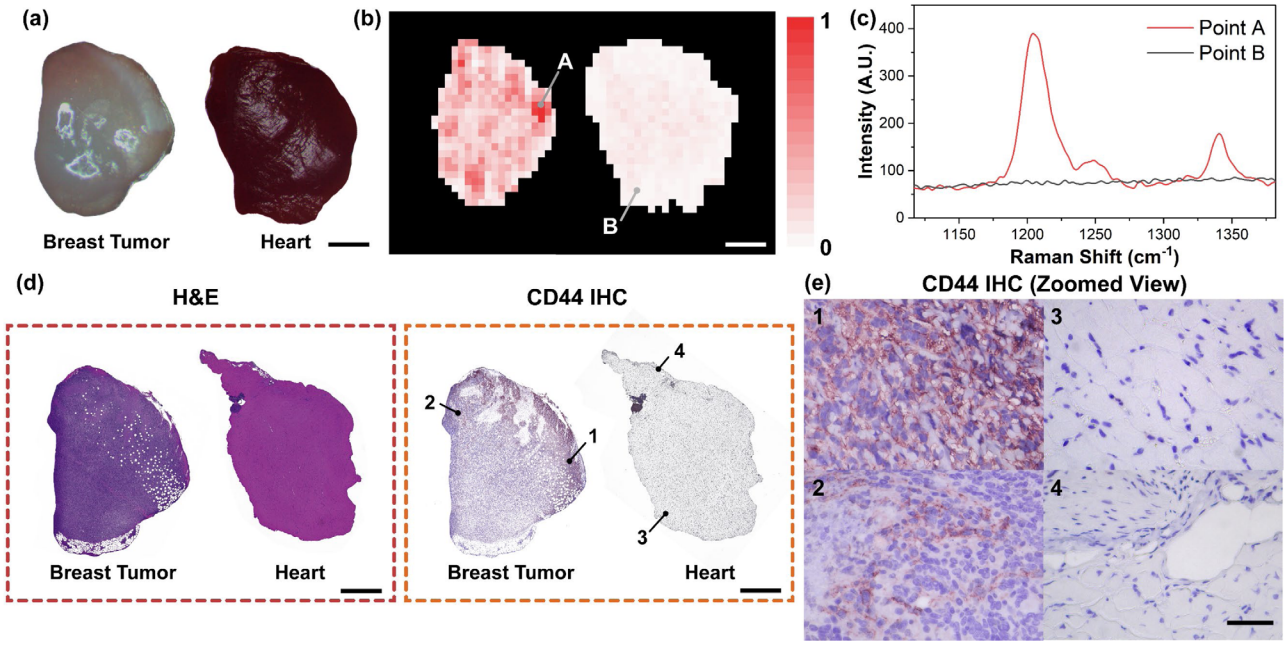

Fig. 4. Imaging results of tissues topically stained with Liposome-S440-HA. Mice breast tumors and hearts serve as positive and negative control groups. (a) Photograph of tissues stained with Liposome-S440-HA. (b) SERS intensity map of the tissues imaged with SNSPD-SSRS; points A and B indicate representative tumor and heart regions. (c) Representative Raman spectra from points A and B in (b). (d) H&E and CD44 IHC-stained histology images of the same tissues, captured at 10× magnification. Points 1–4 mark the representative regions of CD44 IHC images. (e) Enlarged (40×) CD44 IHC images of regions highlighted in (d), showing only CD44 expression in tumor tissues. Scale bar: 2 mm for (a)–(d) and 50 μm for (e).

mouse breast tumor, corroborating the targeting results observed with the SNSPD-SSRS system. Whole-slide scans acquired using a commercial microscope with a 10× objective lens are presented in Fig. 4(d). The morphology observed from these slides closely matches the Raman intensity maps obtained from the SNSPD-SSRS. Figure 4(e) shows some zoomed-in regions of the IHC-CD44 slides acquired with 40× objective lens. In these images, CD44-positive areas appear as brown staining, which is highly concentrated in tumor tissue but absent in the control heart tissue. These results further confirm the targeting specificity and detection accuracy of the SNSPD-SSRS system in distinguishing tumor tissue from healthy tissue, highlighting its potential for precise and sensitive cancer detection.

Overall, these experimental results demonstrated the high-sensitivity imaging capabilities of the SNSPD-SSRS system, making it a compelling platform for early cancer detections. The tunable laser operates at a safe power level, making it well-suited for future in vivo imaging and potential clinical translation. Additionally, the system's design flexibility allows for expansion by adding ultra-narrow filters and SNSPD devices, thereby broadening its spectral coverage and enabling the detection of additional features.

Future enhancements could further elevate system performance. For instance, acquisition speed could be significantly accelerated by replacing the current tunable laser with a vertical-cavity surface-emitting laser (VCSEL). Alternatively, even without hardware upgrades, narrowing the sweeping range (Fig. S5) can substantially reduce acquisition time. Spectral resolution could also be improved by replacing the existing bandpass filter with a Fabry–Pérot filter. Furthermore, by conjugating SERS NPs with different molecular biomarkers, the SNSPD-SSRS system can achieve multiplexed detection of multiple targets [15]. These advancements would position SNSPD-SSRS as a powerful tool for rapid, large-scale screening across a wide range of cancer types.

Funding. National Science Foundation (1808436, 1918074, 2306708, 2237142-CAREER); U.S. Department of Energy (234402).

Disclosures. The authors declare no conflicts of interest.

Data availability. Data presented in this paper are available upon reasonable request to the corresponding author.

Supplemental document. See Supplement 1 for supporting content.

REFERENCES

1. F. Bray, M. Laversanne, H. Sung, *et al.*, CA Cancer J. Clin. **74**, 229 (2024).
2. A. Mahadevan-Jansen and R. R. Richards-Kortum, J. Biomed. Opt. **1**, 31 (1996).
3. J. Langer, D. J. de Aberasturi, J. Aizpurua, *et al.*, ACS Nano **14**, 28 (2020).
4. H. Shin, B. H. Choi, O. Shim, *et al.*, Nat. Commun. **14**, 1644 (2023).
5. J. Grun, C. K. Manka, S. Nikitin, *et al.*, Anal. Chem. **79**, 5489 (2007).
6. W. F. Herrington, C. Burgner, A. H. Atabaki, *et al.*, Opt. Express **29**, 24723 (2021).
7. E. Parham, A. Rousseau, M. Quémener, *et al.*, Neurophotonics **11**, 025007 (2024).
8. J. Song, P. T. C. So, H. Yoo, *et al.*, J. Biomed. Opt. **29**, S22703 (2024).
9. K. X. E. Kay, A. H. Atabaki, W. B. Ng, *et al.*, J. Raman Spectrosc. **53**, 1321 (2022).
10. M. O. A. Malik, C. M. Hsieh, and Q. Liu, IEEE Trans. Instrum. Meas. **74**, 6002413 (2025).
11. N. Persit, J. Kim, D. Gray, *et al.*, *CLEO: Applications and Technology* (Optica Publishing Group 2021), paper ATh4Q.6.
12. Y. Liu, C.-Y. Yao, T. M. Rambo, *et al.*, Opt. Lett. **49**, 6349 (2024).
13. K. Liu, A. K. M. A. Ullah, A. Juhong, *et al.*, Small Sci. **4**, 2300154 (2024).
14. J. Lesley, V. C. Hascall, M. Tammi, *et al.*, J. Biol. Chem. **275**, 26967 (2000).
15. O. E. Eremina, A. T. Czaja, A. Fernando, *et al.*, ACS Nano **16**, 10341 (2022).